ARTICLE

Check for updates

Unified energy law for fluctuating density wave orders in cuprate pseudogap phase

Rong Li[1] & Zhen-Su She [1 ✉]

The quantum origin of the cuprate pseudogap is a central conundrum of condensed matter physics. Although many symmetry-broken scenarios were previously proposed, universal quantitative relationships have been rarely studied. Here, we report a unified energy law underlying the pseudogap, which determines the scattering rate, pseudogap energy, and its onset temperature, with a quadratic scaling of the wavevector of density wave order (DWO). The law is validated by data from over one hundred samples, and a further prediction that the master order of pseudogap transforms from fluctuating spin to charge DWO is also confirmed. Furthermore, the energy law enables our derivation of the well-known linear scalings for the resistivity of the strange metal phase and the transition temperature of the superconducting phase. Finally, it is concluded that fluctuating orders provide a critical bridge linking microscopic spectra to macroscopic transport, showing promise for the quantification of other strongly correlated materials.

---

[1] State Key Laboratory for Turbulence and Complex Systems, College of Engineering, Peking University, 100871 Beijing, China. ✉email: she@pku.edu.cn

A central puzzle of high-temperature cuprate super-conductors is the pseudogap Δ^* that occurs below a characteristic temperature T^*, manifested by suppressing the electronic density of states around the Fermi level[1,2]. The critical question that remains unanswered is, what is the underlying quantum order that determines the pseudogap? Experimentally, in the pseudogap phase, two distinct classes of orders are widely reported[1,3–5], namely, zero wavevector $Q = 0$ states (e.g., nematicity, loop current and Cooper pair) and the finite wavevector $Q \neq 0$ density wave order (DWO). From a mean-field viewpoint, the DWO breaks translational symmetry to produce an anisotropic gap, and small Fermi surface (FS) pockets[1,6,7]. However, experimentally observed static (mainly short-range) DWOs exhibit an onset temperature significantly lower than T^* and no further gap opening[1,2], apparently ruling out the static DWO as the origin of the pseudogap[3,8]. On the other hand, the nematic and loop current orders are observed to emerge coincidentally during the pseudogap opening at T^* [4,5]. However, within the mean-field theory, these intra-unit-cell orders are known to be unable to break the lattice translation symmetry to open a pseudogap[9,10]. Thus, the controversy of whether the pseudogap opening can be related to the conventional form of these two classes[1] remains to be solved.

Recent theoretical advances suggest that the pseudogap phase can be understood with intertwined orders, including the $Q \neq 0$ DWO and the $Q = 0$ nematic, loop-current or superconducting states[8,9,11–13]. For instance, it was demonstrated that a partially melted unidirectional DWO (either spin or charge) could generate a vestigial nematic phase[13]. In this context, using elaborate data analysis, various experiments were performed to achieve precise measurements of energy scales and wavevectors associated with a charge density wave (CDW), revealing an intimate link among CDWs, the nematic order, and the pseudogap. Specifically, recent Raman measurements of the spectral gap associated with CDWs (Δ_{CDW}) in $Bi_2Sr_2CaCu_2O_{8+\delta}$ (Bi-2212), $HgBa_2CuO_{4+\delta}$ (Hg-1201), $HgBa_2Ca_2Cu_3O_{8+\delta}$(Hg-1223) and $YBa_2Cu_3O_{6+\delta}$(Y-123), display the same doping dependence as the pseudogap energy[14,15], indicating that the pseudogap and the CDW energy scale may have a common microscopic origin. Furthermore, by analysing tunnelling conductance from distinct regions of momentum space, Mukhopadhyay et al. identified energies characterizing the CDW, nematicity, and pseudogap in Bi-2212 and found that they are identical[16], which suggested that the pseudogap may originate from highly disordered unidirectional DWO. This viewpoint was further supported by more recent observations from scanning tunnelling microscopy (STM) and nuclear magnetic resonance (NMR): the CDW phase is locally unidirectional (with significant phase fluctuations globally) for underdoped Bi-2212[17–19] and Y-123[20], and the local spectral gap in $(Bi,Pb)_2(Sr,La)_2CuO_{6+\delta}$ (Pb-Bi2201) is positively correlated with fluctuating CDW wavevector[21].

While the above-mentioned theoretical and experimental progress indicates a mainly qualitative link between the CDW and the pseudogap and highlights the crucial role of phase fluctuations (either thermal fluctuations or spatial disorders) in this link, we are devoted to investigating whether there exists a universal quantitative relationship between energy scales of the pseudogap and the fluctuating DWO. In this context, three critical challenges remain to be addressed[15,22]. First, one needs to define the energy scales linked to the intrinsic nature of DWO to determine whether the measured gap is from the CDW rather than other orders. Second, one needs to have a clear explanation for the origin of the universal doping dependence of Δ^* and T^*. Finally, one needs to explain the transition from a CDW to a spin density wave (SDW) and its influence on the pseudogap[1,23,24]. To answer these questions, we naturally introduce the wavevector

and amplitude as the two fundamental quantities to characterize DWO and to investigate their relationships with two critical energy scales in the single-particle self-energy (see the "Methods" subsection "Characteristic energy scales and the DWO order parameter"), namely, the gap energy and the scattering rate.

To derive these relationships, we use an innovative symmetry-breaking analysis inspired by a recent successful wall turbulence theory[25]. This structural ensemble dynamics (SED) theory[25,26] demonstrated that, although wall turbulence encompasses fully spatio-temporal chaotic motions (or eddies), due to shear stress, its time-averaged behaviour, constrained by wall-induced dilation symmetry, is spatially self-organized into several simple ensembles. Within each ensemble, turbulent eddies have their characteristic length size as the crucial similarity parameter, on which momentum transport coefficient has a universal power-law dependence. This theory predicts the energy distribution[26] and transport coefficient[25] over the entire domain. Here, we regard fluctuating DWO below T^* as eddies in wall turbulence, whose statistical behaviours must obey similar self-organized structures dictated by underlying symmetry-braking characterizing the electron–electron correlations in pseudogap phase through an appropriate length. Specifically, as ubiquitously observed in cuprates[3,8,23,27], the mesoscopic (fluctuating) DWO emerges as a consequence of translational symmetry-breaking. Therefore, following SED, we assume that the pseudogap energy scales should satisfy a power-law relation with the wavevector (or wavelength) of the fluctuating DWO. In a microscopic scattering view, its wavelength $l_o = 2\pi/Q_o$ corresponds to a small wavevector Q_o (smaller than the reciprocal lattice vector, where o represents the order type), which connects momentum states on the FS, favouring the Umklapp scattering associated with Q_o to determine the pseudogap energy scales in the single-particle self-energy.

Here, we regard T^* as the onset temperature of the particle–hole pairing that breaks translational symmetry locally and instantaneously, and the transition temperature T_{DW} of quasi-static DWO[27] as the onset temperature of phase coherence, and the dynamic DWO above T^* [28] as amplitude fluctuations of this pairing. Especially, we assume that the highly disordered DWO presented below and near T^* is a particular nematic order that breaks the two-dimensional rotational symmetry on a large scale but maintains the unidirectional DWO locally. Therefore, in this work, we focus on the locally fluctuating unidirectional DWO below T^* (for both the nematic and the quasi-static states), which, we assume, can be described by one-dimensional order parameters with a small-wave vector or low-frequency phase fluctuations.

In the following, we first introduce an Umklapp phason scattering mechanism to derive a quadratic scaling with the DWO wavevector for the scattering rate and further extend it to the pseudogap energy Δ^* and the onset temperature T^*. The scalings are then validated by the spectral gap and the onset temperature data obtained for over one hundred samples, indicating that the universal monotonic decrease with increasing doping of Δ^* and T^* in the intermediate doping regime originates from the variation in the CDW wavevector Q_{CDW}. Furthermore, by using resistivity data of high-quality single crystals, we demonstrate the validity of the quadratic scaling, with a universal scattering coefficient for both the CDW and SDW. Besides, by using the energy law, we can derive a length, from the resistivity and pseudogap energy data (with the so-called length mapping method), of the master order, which displays a universal transition in the pseudogap phase from the SDW (at light doping) to the CDW (at intermediate doping), as confirmed by independent measurements. Finally, the new energy law offers a straightforward explanation for both the strange metal resistivity and the

linear scaling between the superconducting transition temperature and superfluid density, indicating that the law is universal for all three phases of hole-doped cuprates. These findings let us conclude that mesoscopic (fluctuating) orders provide a crucial bridge (in universal energy scaling) linking microscopic spectra to macroscopic transport in cuprates. This discovery offers a potential breakthrough towards a comprehensive theoretical description of strongly correlated materials.

Results

Universal energy law for fluctuating DWO. The fluctuating DWO generates phason modes to induce carrier scattering, which requires conservation of momentum as $\mathbf{k}' = \mathbf{k} + \mathbf{q} + n\mathbf{Q}_o$, where $\mathbf{k}$ and $\mathbf{k}'$ are the initial and final states, $\mathbf{q}$ is the phason wave-vector, and n is a nonzero integer. Ignoring the anisotropy of the scattering rate $\Gamma_{\mathbf{k}}$, we consider only the mean scattering rate Γ, which is independent of $\mathbf{k}, \mathbf{k}'$, and $\mathbf{q}$ but closely related to Q_o in an Umklapp scattering process. This yields an energy law for the mean scattering rate as follows:

$$\Gamma = \gamma_\Gamma \frac{\hbar^2 Q_o^2}{m^*} = \gamma_\Gamma \frac{h^2}{m^* l_o^2}, \tag{1}$$

where γ_Γ is a dimensionless coefficient describing the mean scattering strength and m^* is the effective mass of a carrier.

Eq. (1) is not only the most straightforward explicit function of $\Gamma(Q_o)$ with correct dimensionality and inversion symmetry but also a natural result of the Umklapp scattering theory under the small momentum difference and a long-wavelength approximation (see the "Methods" subsection "Umklapp scattering rate associated with DWO"). The scattering theory also predicts that γ_Γ is proportional to the module square of the carrier–DWO coupling. Based on a simple energy correspondence to the $t - J$ model[29], we assume that this coupling is proportional to the ratio between the superexchange energy J and the hopping energy t, which yields:

$$\gamma_\Gamma = F_\Gamma \frac{J^2}{t^2} \approx 0.11 F_\Gamma, \tag{2}$$

where the dimensionless coefficient F_Γ is proportional to the square of the fluctuating DWO amplitude A, i.e., $F_\Gamma \propto A^2$. The second equality originates from the approximation $J/t \approx 1/3$, supported by ab initio calculations and Raman scattering data[30,31]. Generally, F_Γ may depend on temperature and doping. However, recent spectroscopy experiments reveal that the dynamical charge and spin excitations pervading the phase diagram of cuprates and their scattering energy (e.g., peak locations and intrinsic width) are little affected by temperature and doping in the pseudogap phase[28,32,33]. These findings reveal that in the intermediate temperature and doping regime discussed below (see also the "Discussion" section), the temperature and doping contributions may be renormalized. Based on these experimental observations, we assume F_Γ and γ_Γ away from quantum critical points to be doping and temperature-independent and let the experimental data determine their magnitudes.

Furthermore, as for the scattering rate, we propose that the characteristic gap amplitude Δ originates from the Umklapp scattering by the fluctuating DWO. Therefore, Δ can be predicted from Eq. (1) by extending the scattering source from order fluctuations to its mean-field, which involves only the substitution of the amplitude of phason modes at $q \neq 0$ in Eq. (2) for the amplitude of modes at $q = 0$ without further calculations. Thus,

we obtain an energy law similar to Eq. (1):

$$\Delta = \gamma_\Delta \frac{\hbar^2 Q_o^2}{m^*} = \gamma_\Delta \frac{h^2}{m^* l_o^2}, \tag{3}$$

Here, $\gamma_\Delta = F_\Delta J^2/t^2 \approx 0.11 F_\Delta$ is the dimensionless coefficient describing the scattering strength, where F_Δ is a dimensionless parameter proportional to the square of the mean-field amplitude. Similarly, we assume F_Δ and γ_Δ below and away from T^* to be doping and temperature-independent and let the experimental data determine their magnitudes.

From a pairing perspective, the DWO is equivalent to pairing in the particle–hole channel[34]. In this context, we define the onset temperature T^* of the pseudogap opening with the emergence of this particle–hole pairing. This implies that the thermal-fluctuation energy $k_B T^*$ is linearly proportional to the pseudogap energy, as widely observed in spectroscopic measurements[15,35]. This naturally yields a relationship for determining T^*, as follows:

$$T^* = \gamma_T \frac{\hbar^2 Q_o^2}{m^*} = \gamma_T \frac{h^2}{m^* l_o^2}, \tag{4}$$

where $\gamma_T \propto \gamma_\Delta$ is a dimensionless coefficient. In addition, in the following, we express Q_o in units of $2\pi/a_0$, where a_0 is the in-plane lattice constant.

Gap energy scales associated with the CDW. The CDW has been identified as a leading competitor of superconductivity in cuprates[3]. Therefore, it would be intriguing to examine Eqs. (3) and (4) to evaluate whether the CDW is indeed related to the pseudogap and satisfies these simple energy laws. Recently, using STM, Webb et al. carried out simultaneous measurements of the spectral gap and Q_{CDW} for local charge modulations in $(\text{Bi, Pb})_2(\text{Sr, La})_2\text{CuO}_{6+\delta}$ (Pb-Bi2201) at a superconducting state (at 6 K)[21], providing an appropriate sample for this evaluation. Taking $m^* = 2.7 m_e$ (m_e is the electron mass) for Bi-2201 based on the optical conductivity measurement[36] and $\gamma_\Delta = 0.135$, Eq. (3) were used to predict a quadratic scaling, $\Delta = \hbar^2 Q_{CDW}^2/20 m_e$, that is quantitatively consistent with the majority of the reported data shown in Fig. 1. This agreement confirms the quadratic scaling between Δ and Q_{CDW}.

It is interesting to compare the present prediction with previous theories. In the past, the connection between the pseudogap and Q_{CDW} was attributed to fermiology, which explains the decrease in Q_{CDW} with increasing doping as a result of a growing hole pocket[37,38]. The predictions of two models based on this fermiology[21] are presented in Fig. 1. In the antinodal (AN) case, Q_{CDW} connects the nested AN segments of the FS, and in the antiferromagnetic zone boundary (AFZB) case, Q_{CDW} connects the points at which the FS crosses the AFZB. Both models show apparent overestimation for the optimal and underdoped regimes. Therefore, the present proposal that the spectral gap associated with CDW originates from scattering by CDW rather than the simple FS instability is well confirmed. As discussed in previous studies[21,37], the failure of these simple Fermiology may be the neglect of the renormalization of strong interactions, which is captured in the present theory. In addition, one may wonder whether the global incommensurability is compatible with recent STM and NMR observations that the CDW is locally commensurate for underdoped Bi-2212 and Y-123[17–20]. Assuming phase fluctuations to be of Gaussian type, we derive from Eq. (3) a gap distribution that is quite similar to the experimental observations (see Supplementary Note 2), implying that the present energy law applies to the locally commensurate CDW and the accompanying phase fluctuations.

Note that, the spectral gap in Fig. 1 is defined as the peak location of the differential conductance spectra of the low-temperature (6 K) superconducting phase. Therefore, it may
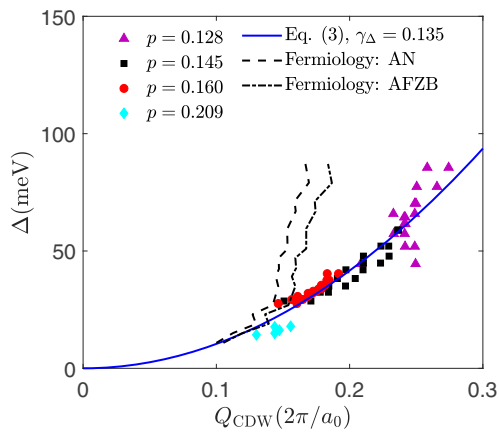
Fig. 1 Scaling between the spectral gap and the charge density wave (CDW) vector. The symbols represent the spectral gap (Δ) and the CDW vector (Q_{CDW}) data in Pb-Bi2201 of the low-temperature (6 K) superconducting phase determined from scanning tunnelling microscope measurements[21], and a_0 is the in-plane lattice constant. The solid blue line represents the prediction from Eq. (3) with the scattering parameter $\gamma_\Delta = 0.135$ and the effective mass $m^* = 2.7 m_e$, where m_e is the electron mass. The root mean squared error is 6 meV. The dashed and dash-dotted lines represent the Fermiology-driven wavevectors[21], i.e., the antinodal (AN) case and the antiferromagnetic zone boundary (AFZB) case, respectively.
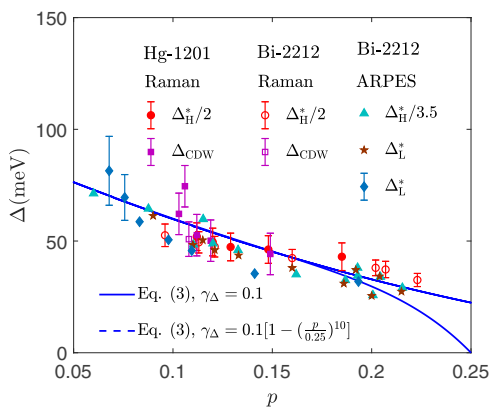

Fig. 2 Doping (p) dependence of various gap energy scales (Δ). The symbols represent the low-(Δ_L^*) and high-(Δ_H^*) energy scales of the pseudogap and the charge density wave (CDW) gap (Δ_{CDW}) of Hg-1201 and Bi-2212 determined from the Raman response[15] and the angle-resolved photoemission spectroscopy (ARPES) data[35,42]. The vertical errors are extracted from the previous measurements[15,35,42]. The solid blue line represents the prediction from Eq. (3) with the scattering parameter $\gamma_\Delta = 0.1$ and the effective mass $m^* = 2.45 m_e$ (m_e is the electron mass), a linear model $Q_{CDW} = 0.343 - 0.699p$ of the CDW vector and the in-plane lattice constant $a_0 = 3.89$ Å for Hg-1201[94]. The dashed blue line includes a quick decay of the CDW amplitude near the pseudogap quantum critical point. The root mean squared error for solid and dashed lines are both 6 meV.

represent a composite gap synthesized contributions of both the CDW and the superconducting gaps. Thus, it is important to find a way to distinguish these gaps. The recent Raman response measurements[14,15] defined the CDW gap (Δ_{CDW}) as the nodal hump location persisting above the superconducting transition temperature T_c, the high-energy scale pseudogap Δ_H^* as the AN depletion location above T_c, as shown in Fig. 2. Interestingly, with simple normalizations (i.e., divide energy by constant), the

experimental data for both gaps in Hg-1201 (hollow symbols) and Bi-2212 (solid symbols) collapse to the solid blue line predicted by Eq. (3). The fitting parameters are $\gamma_\Delta = 0.1$, $m^* = 2.45 m_e$ (determined from the quantum oscillation experiment of Hg-1201 at $p = 0.09$[39]) and $Q_{CDW} = 0.343$–$0.699p$ (linearly fitted from the experimental data for Hg-1201[40,41]; see Supplementary Note 1). On the other hand, the angle-resolved photoemission spectroscopy (ARPES) measurement in the AN direction usually suggests two energy scales for the pseudogap, namely, the low-energy scale (Δ_L^*, e.g., the peak location) and the high-energy scale (Δ_H^*, e.g., the hump location)[42]. It is remarkable that both energy scales for Bi-2212 determined from ARPES measurement[35,42] follow the doping dependence of our prediction as well.

Figures 1 and 2 contain three types (STM, Raman, and ARPES) of data for over 50 samples of three compounds; thus, our theory is firmly validated. In addition, since the pseudogap onset temperature is the gap opening temperature, T^* should also satisfy the same quadratic scaling. As shown in Fig. 3, the predictions from Eq. (4) are indeed consistent with experimental data over a wide doping range of Bi-2201, Bi-2212 and Hg-1201[15,43], confirming the universality of the energy law. Note that in the fitting of Bi-2201, a power-law model $Q_{CDW} = 0.269[1 - (p/0.261)^{3.79}]$ fitted from the previously reported experimental data[24,44] has been used (see Supplementary Note 1).

Our findings reveal that, in the CDW-dominated regime, the well-known monotonic decreases in Δ and T^* for three compounds with short-range DWOs mainly result from the reduction of the CDW wavevector with increasing doping. Furthermore, our theory enables us to propose a preliminary explanation for the origin of the high-energy pseudogap, i.e., Δ_H^*. Specifically, we assume that Δ_H^* originates from the multi-fold scattering rather than the one-fold scattering process of the low-energy pseudogap. For instance, the coupling of x-directional and y-directional one-fold scattering by unidirectional CDWs (with wave vectors $|\mathbf{Q}_x| = |\mathbf{Q}_y| = Q_{CDW}$) results in two-fold pseudogap energy, i.e., $\gamma_\Delta \hbar^2 |\mathbf{Q}_x + \mathbf{Q}_y|^2 / m^* = 2\Delta_{CDW}$, which then provides a natural explanation for the high-energy pseudogap of Raman data. Besides, the early-stage ARPES measurements[42] determined higher pseudogap energy than the Raman response, for it defined the gap with raw data without subtracting the high-temperature signal, which we suspect may also be explained by higher-fold scattering processes. A thorough theoretical description of the high-energy process with a multi-fold scattering scenario will soon be communicated in the future. Note also that the experimental data begin to deviate from the prediction at $p \sim 0.2$, likely because the CDW amplitude begins to decrease noticeably near the pseudogap quantum critical point (QCP), which might be described by the defect power law of γ_Δ (the dashed blue lines in Figs. 2 and 3). Furthermore, near $p \sim 1/8$, T^* for Bi-2212 and Hg-1201 is lower than our prediction, which may reveal an anomaly in the CDW gap opening. Its relevance to the temperature and doping variations of the CDW amplitude and the effective mass (assumed to be doping independent here) should be investigated in the future.

Characteristic resistivity associated with a CDW. Despite considerable discussion on the contribution of CDWs to the electronic spectrum[6,9,34,45,46], the connection between CDWs and charge transport is rarely mentioned because of the difficulty in associating the scattering rate with the CDW. However, our phenomenology provides a simple way to make this connection. Generally, transport dissipation stems from a substantial momentum transfer (e.g., backward scattering), which is a subset of all-microscopic scattering processes[47]. Thus, we assume that the (macroscopic) transport scattering rate is proportional to but
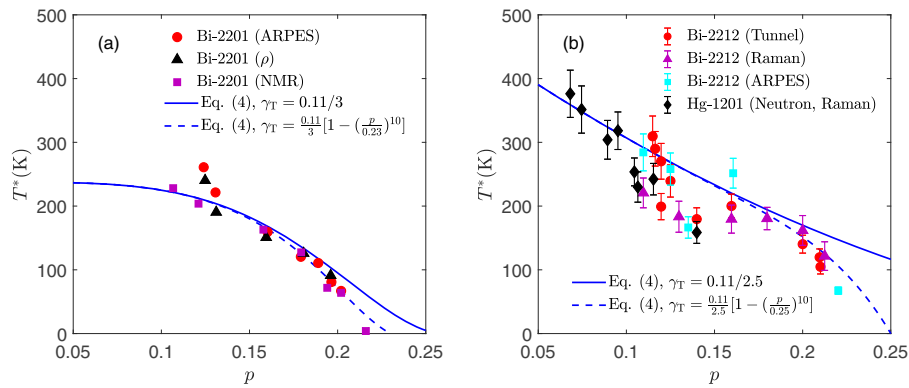
Fig. 3 Doping (p) dependence of the pseudogap onset temperature T^*. a The symbols represent Bi-2201 data determined from previously reported measurements[43]. The solid blue line represents the predictions from Eq. (4) with the scattering parameter $\gamma_T = 0.11/3$, the effective mass $m^* = 2.7m_e$ (m_e is the electron mass), and a power-law model $Q_{CDW} = 0.269[1 - (p/0.261)^{3.79}]$ of the charge density wave (CDW) vector. The root mean squared error for solid and dashed lines are 30 and 20 K, respectively. **b** The symbols represent Bi-2212 and Hg-1201 data determined from previously reported measurements[15]. Besides, the vertical errors are extracted from these measurements[15] as well. The solid blue line represents the prediction from Eq. (4) with $\gamma_T = 0.11/2.5$, $m^* = 2.45m_e$, and $Q_{CDW} = 0.343 - 0.699p$. The dashed blue lines indicate the quick decay of the CDW amplitude near the pseudogap quantum critical point. The root mean squared error for solid and dashed lines are 50 and 40 K, respectively. The acronyms ARPES, ρ, NMR, Tunnel, Raman, Neutron in the figure legends represent the data from angle-resolved photoemission spectroscopy, resistivity, nuclear magnetic resonance, tunnelling, Raman and neutron experiments, respectively.
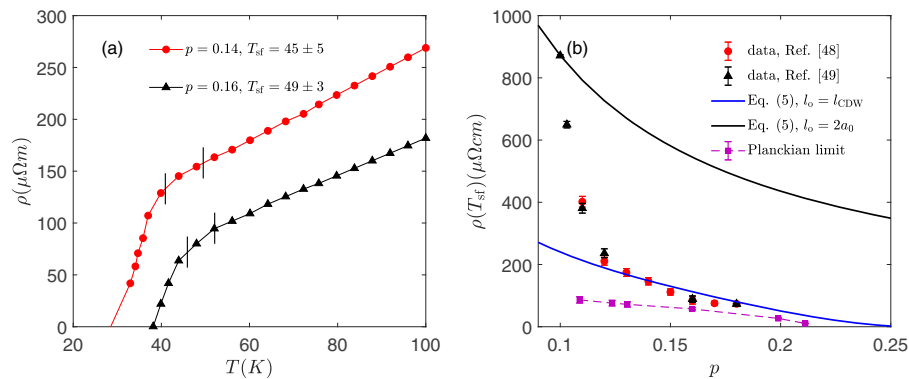

Fig. 4 Characteristic resistivity at the onset temperatures (T_{sf}) of the SC fluctuations in Bi-2201. a The temperature (T) dependence of the resistivity (ρ). The symbols represent the experimental data obtained by Ando et al.[48]. The pairs of vertical lines indicate the T_{sf} error bars determined from the specific-heat measurement[95]. **b** Doping (p) dependence of $\rho(T_{sf})$. The red and black symbols represent the experimental values determined from previously reported measurements[48,49]. The vertical errors are estimated from the resistivity variation associated with the T_{sf} error bars. The solid blue line represents Eq. (5) prediction with the scattering parameter $\gamma_\Gamma^* = 0.11$ and the charge density wave (CDW) period l_{CDW}, which is compared to the prediction (solid black line) with the antiferromagnetism period length $2a_0$, as well as the predictions (purple squares) from Planckian dissipation theory[50] with the effective mass $m^* = 2.7m_e$ (m_e is the electron mass) and T_{sf}. The root mean squared error of the solid blue line fit to data above $p = 0.12$ is 20 $\mu\Omega$ cm.

smaller than the (microscopic) single-particle scattering rate, $\hbar/2\tau = C_\tau\Gamma$, where τ is the relaxation time and C_τ is a dimensionless coefficient <1. By substituting τ and Eq. (1) into the Drude model, we obtain the in-plane resistivity:

$$\rho_o = \gamma_\Gamma^* \frac{R_Q}{n_c l_o^2}, \qquad (5)$$

where $\gamma_\Gamma^* = 4\pi C_\tau\gamma_\Gamma$, $R_Q = h/e^2$ is the quantum resistance, $n_c = pK/a_0 b_0 c_0$ is the carrier density, a_0 and b_0 are the in-plane lattice constants, c_0 is the c-axis lattice constant, K is the number of Cu or Fe ions in one unit cell, and p is the carrier concentration per ion.

Equation (5) quantifies the characteristic resistivity determined by DWO fluctuations. A good candidate for the verification is the underdoped Bi-2201 because its short CDW correlation length fluctuates between 0.75 and 1.5 times the CDW period l_{CDW}[44], which may efficiently induce scattering. We extract the characteristic resistivity of CDW scattering from previously reported data obtained from high-quality single crystals[48,49],

which have very small residual resistivity at optimum doping. During the extraction, we cautiously avoided the influence of superconductivity (SC) by selecting the "knee" data $\rho(T_{sf})$ at the onset temperature T_{sf} of the SC fluctuations, as presented in Fig. 4a.

In Fig. 4b, we fit $\rho(T_{sf})$ with Eq. (5) and the CDW period length $l_{CDW} = 2\pi/Q_{CDW}$, where Q_{CDW} is estimated with the same power law, $0.269[1 - (p/0.261)^{3.79}]$, used in Fig. 3a. We find that a constant scattering coefficient $\gamma_\Gamma^* = 0.11 \approx J^2/t^2$ makes the predictions agree well with the data from 10 samples between $p = 0.12$ and 0.18[48,49]. This outcome is consistent with the presence of CDW ordering in the $p = 0.11 - 0.16$ region observed by resonant inelastic X-ray scattering[44]. Quantitatively, when the doping increases from 0.12 to 0.18, l_{CDW}^2 increases by 80%, which is higher than the 50% increase in the carrier density, revealing that the decrease in $\rho(T_{sf})$ is dominated by the variation in the CDW period length.

It would be helpful to compare the present analysis with other theoretical approaches. In Planckian dissipation theory[50,51], the

scattering rate solely determined by temperature is $\hbar/\tau = k_B T$, which predicts the resistivity at T_{sf} to be $\rho(T_{sf}) = (m^*/n_c e^2)(k_B T_{sf}/\hbar)$. Taking $m^* = 2.7 m_e$ from optical conductivity measurements[36], this prediction (Fig. 4b, purple squares) underestimates the data by nearly 50%. One way to remedy this discrepancy is to attribute it to the "residual resistivity" induced by impurities. However, the stochastic nature of impurities makes the minimum residual resistivity of optimally doped cuprates difficult to explain[52,53]. Therefore, the above results reveal that the "knee" resistivity at T_{sf} in the pseudogap phase has a simple scaling of $\rho(T_{sf})n_c \propto l_{CDW}^{-2} \propto Q_{CDW}^2$ and thus satisfies the energy law of Eq. (1).

Universal sheet resistance for an antiferromagnetic SDW. An antiferromagnetic (AF) SDW is another widespread DWO in the underdoped regime of HTSCs. Thus, it would be intriguing to examine Eq. (5) to determine whether the AF SDW satisfies the energy law of Eq. (1). In both cuprate-based and iron-based HTSCs, the phase transition between AF and SC is characterized by a low-temperature plateau for the resistivity[49,54], as shown in Fig. 5a. In a superconductor–insulator (SI) transition scenario, the corresponding sheet resistance is predicted to be a universal value, namely, $h/4e^2 = 6450\,\Omega$ in the Boson localization theory[55]. However, experimental observations revealed that the critical resistance is sample-dependent within a factor of 0.5–2 of the predicted values, which motivated Goldman's question: "What different physical models govern the various SI transitions which have different critical resistances?"[55]. We now provide a quantitative explanation for this sample-dependent resistance, using Eq. (5).

In our theory, the plateau is attributed to the Umklapp scattering by characteristic fluctuations of the AF SDW with $l_o \approx 2a_0$. By substituting this l_o into Eq. (5), we predict the critical sheet resistance as follows:

$$R_\square = \frac{\rho}{c_0/K} = \frac{\gamma_\Gamma^*}{p_c}\frac{h}{4e^2}, \tag{6}$$

where γ_Γ^* is the corresponding scattering coefficient and p_c is the critical carrier concentration. If γ_Γ^* is universal, then Eq. (6) predicts that $R_\square$ is inversely proportional to p_c. As shown in Fig. 5b, the prediction with a constant $\gamma_\Gamma^* = 0.11$ is quantitatively consistent with the reported data for both hole-doped cuprates and iron pnictides within a wide doping range.
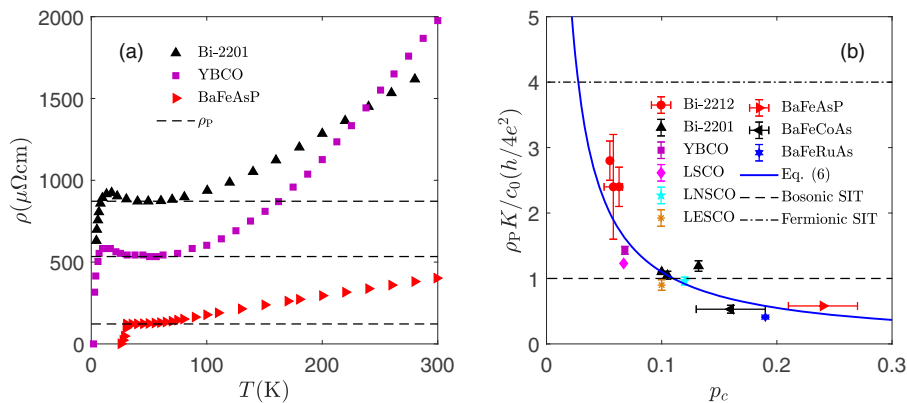
The validation of Eq. (6) yields a surprising prediction that the critical sheet resistance per carrier is a universal value, $R_\square p_c = \gamma_\Gamma^* h/4e^2 \approx 710\,\Omega$, which represents the true universal feature behind observed critical resistances. This universal sheet resistance of $710\,\Omega$ per carrier is not present in the total resistance description ($R_\square$) by the localization theory[55], and we have achieved a good answer to Goldman's question. Furthermore, since the parents of iron pnictides are metals but not insulators, the validity of Eq. (6) above implies that the energy law is applicable for AF fluctuations in both AF insulator and metal states.

Transition from a CDW to an SDW. It is well known that decreasing doping in cuprates induces an order transition from charge to spin sectors[1,56]. Remarkably, the present theory fully confirms this transition from a fluctuating CDW at intermediate doping to an SDW at light doping in the validations of Eqs. (5) to (6) in Figs. 4 and 5. Specifically, Eq. (5) enables us to quantify DWO's period length from resistivity data: $l_o = \sqrt{\gamma_\Gamma^* R_Q / \rho(T_{sf}) n_c}$, where $\rho(T_{sf})$ is observational data. As shown in Fig. 4b for Bi-2201, as the doping decreases, $\rho(T_{sf})$ increases sharply from $236\,\mu\Omega\,cm$ at $p = 0.12$ to $871\,\mu\Omega\,cm$ at $p = 0.10$. Taking $\gamma_\Gamma^* = 0.11$, the sharp increases in $\rho(T_{sf})$ is explained by an order's period change from $l_{CDW} \approx 4a_0$ to $l_{SDW} \approx 2a_0$, which indicates a possible transition from a CDW-dominated regime to an AF SDW-dominated regime. This assertion is remarkably consistent with an observation from NMR measurements[57] that suggests that the CDW supersedes AF near $p = 0.11$ in Bi-2201.

In addition to the consistency for the above-predicted order transition from a CDW to an AF SDW, let us further investigate whether it can also describe the transition in the pseudogap energy scale. Recently, STM measurements of Bi-2201 have exhibited a monotonic increase in the gap energy from $p = 0.12$ to $p = 0.03$, and the absence of a CDW at $p = 0.03$[24]. The latter suggests that there must be another order dominating the gap in the lightly doped AF regime. According to our theory, SDWs have a larger wavevector (near 0.5) than CDWs (near 0.25), resulting in a larger energy gap, and this finding is qualitatively consistent with the STM observation. Quantitatively, taking $l_o = 2a_0$ (the AF period), $\gamma_\Delta = 0.135$ (the same value as Pb-Bi2201) and $m^* = 2.2 \pm 1 m_e$ (from optical conductivity

Fig. 5 Critical resistance near the antiferromagnetism–superconductivity transition. a The temperature (T) dependence of the resistivity (ρ). The symbols represent experimental values with a low-temperature plateau (ρ_P, dashed lines) near critical doping, determined from previously reported measurements[48,49,54]. **b** Critical sheet resistance of the plateau. The symbols represent the plateau values determined from previously reported experimental data[48,54,95-99] (see Supplementary Note 5), where K is the number of Cu or Fe ions in one unit cell, c_0 is the c-axis lattice constant, h/e^2 is the quantum resistance unit. The vertical errors are estimated from the plateau-determination uncertainty, and the horizontal errors are estimated from the concentration-determination uncertainty. The solid blue line represents the prediction from Eq. (6) with the scattering parameter $\gamma_{SDW}^* = 0.11$ and carrier densities and lattice constants[54,93,96,98,100-102]. The root mean squared error of the solid blue line is $0.4h/4e^2$. The dashed and the dash-dotted lines represent the Boson and Fermion localization theories for the SI transition (SIT)[55].

measurements at $p = 0.03$[36]), we predict that $\Delta^* = 170$–470 meV, which is close to the gap energy scale (i.e., 400–600 meV) measured by STM at $p = 0.03$. Note that this estimation is much higher than that measured by STM for the CDW ($\lesssim 100$ meV), which concludes that the pseudogap in the lightly doped regime is indeed determined by the AF SDW.

A further question that our theory should address is whether the CDW extends into the overdoped regime or the energy law is valid across the whole doping range of cuprates[3]. Equation (3) enables the derivation of DWO length $l_o = h\sqrt{\gamma_\Delta / \Delta^* m^*}$ from the pseudogap energy scale using spectroscopic data. While the pseudogaps in Bi-2201, Bi-2212, and LSCO are experimentally shown to persist up to a high doping level of $p = 0.20$–0.22[2,15,21,58], our length mapping formula predicts the existence of CDWs in overdoped cuprates accompanying the pseudogap, consistent with recent STM and RXS measurements of Bi-2201 (up to $p = 0.23$)[44] and LSCO (up to $p = 0.21$)[59]. On the other hand, Eq. (5) enables us to confirm CDW's dominance from resistivity data for overdoped cuprates, such as Y-123[60], Tl$_2$Ba$_2$CuO$_{6+\delta}$[61] and La$_{2-x}$Ce$_x$CuO$_4$[62], for which the predicted l_o in $p = 0.16$–0.22 increases from $3a_0$ to $5.5a_0$. The latter coincides with the characteristic CDW period $l_{CDW} \approx 4a_0$, indicating the possible presence of a dynamic CDW in the overdoped regime. Furthermore, the transport scattering rate of the typical CDW is $\hbar/2\tau = \pi\gamma_\Gamma^* h^2 / m^* l_{CDW}^2 \approx 4.6$ meV with $l_{CDW} = 4a_0$ and $m^* = 2.5 m_e$. These findings are highly consistent with Arpaia et al.'s observations that the short-range dynamical charge density fluctuations are characterized by energies of a few meV, and pervade a large area of the phase diagram[28].

Then, it is of interest to verify these predictions in other strongly correlated materials using the length mapping formula. A preliminary examination has already yielded consistent outcomes. For instance, from Eq. (3) with $\gamma_\Delta = 0.135$ and $m^* = 4 m_e$[63], we predict the charge order length for iridate from the pseudogap amplitude data (i.e., 70–300 meV) to be $l_o = 1.7$–$3.6a_0$, consistent with the STM measurement[64].

Conclusion

In summary, complementary to current theories focusing on intertwined mechanisms of various orders[8,9,11–13], we here uncover a universal energy law linking the pseudogap and the DWO, namely, all three pseudogap energy scales (the scattering rate, the pseudogap energy, and its onset temperature) have a quadratic scaling with the DWO wavevector. All (more than one hundred) single-crystal sample data fully support the present energy law, revealing that the pseudogap originates from the fluctuating DWO, i.e., an SDW at light doping and a CDW at intermediate doping. In our opinion, the universal energy law (and scattering coefficients) represents the zeroth-order relationship between pseudogap energy scales and the DWO wavevector for doping dependence, which provides an important reference point to resolve several conundrums associated with the pseudogap origin.

First, the onset temperature of the pseudogap, if defined as the emergence for the particle–hole pairing of fluctuating SDWs or CDWs, would be naturally higher than the onset temperature of static (coherent) SDWs or CDWs. Second, the universal monotonic decrease in Δ^* and T^* with increasing doping stems from the variation in the amplitude and the wavevector of the SDW and CDW. At light doping, the decreases in Δ^* and T^* are due to a reduction in the amplitude of the SDW, supported by the observation that the antiferromagnetic spectral weight decreases with doping[23]. On the other hand, at intermediate doping, the decreases are due to reductions in the Q_{CDW} and the CDW amplitude, which

is supported by spectroscopic measurements[27,44], as shown in Figs. 2 and 3 for Bi-2201, Bi-2212 and Hg-1201.

Discussion

In contrast, the La-based cuprates exhibit a weak increase in Q_{CDW} with doping (observed in $p = 0.115$–0.21)[27,56,59,65,66] as a consequence of mutual locking of long-range spin and charge orders at low temperatures[65,67,68], a situation that never occurs in other cuprates. Based on a simple analysis of the resistivity (Fig. 5b) and gap data (Supplementary Table 3), we find that the main predictions (e.g., Eqs. (3) and (6)) in this work hold for independent SDW and CDW in the La-based cuprate, but γ_Δ and γ_Γ^* have different values and doping dependencies (see also Supplementary Note 6). It reveals that the decreases in Δ^* and T^* with increasing doping in the CDW-dominated regime for this exceptional class might be due to the reduction of the CDW amplitude, which is preliminarily observed by the decreasing peak height intensity of X-ray diffraction with doping[59]. However, the intertwining effects of spin and charge DW in striped order are neglected in this work and should be further studied in the future.

Furthermore, one may wonder why the CDW transition temperature (T_{CDW}) does not follow the CDW gap (Δ_{CDW}) and onset temperature (T^*) as shown in previously reported measurements[14,15]. Although the clarification of the specific physical mechanism underlying this difference goes beyond the scope of this paper, the present work inspires a preliminary understanding. Specifically, we conjecture that in contrast to Δ_{CDW} and T^* determined by the particle–hole pairing energy, T_{CDW} represents the phase coherence (perhaps local for the short-range charge order) energy of the pairing. If this is correct, there may be a positive correlation between T_{CDW} and the CDW's correlation length characterizing the phase coherence strength. Indeed, this positive correlation is consistent with RXS experiments of Hg-1201[40], Bi-2201[37], YBa$_2$Cu$_3$O$_x$[69] and La$_{2-x}$Sr$_x$CuO$_4$[59,66]. Therefore, we propose that the T_{CDW} dome has an intimate relationship with the phase coherence energy of CDW, which is an intriguing conjecture worth further study.

The present work reports two universal scattering coefficients for the low-energy pseudogap and resistivity, i.e., $\gamma_\Delta \approx \gamma_\Gamma^* \approx J^2/t^2 \approx 0.11$. It is essential to discuss the doping range for the universality of these two scattering coefficients. Our preliminary understanding is that the universality is preserved for compounds with short-range DWO in the intermediate doping regime away from both the AF insulating phase and the pseudogap QCP. The reason is that the AF insulator contains long-range AF correlations, leading to stronger scattering behaviour than short-range fluctuations. In contrast, the pseudogap QCP yields a significant decrease in the DWO amplitude, resulting in a weakening of the scattering. As explained in the "Methods" section, we presently use data from high-quality single crystals with the least degree of impurity among all reported data associated with the same compound. However, our theory may be extended to discuss data obtained for less pure samples[70,71] to quantify the additional impurity effect (see Supplementary Note 3). Note that long-range ordering effects in Y-123 and La-based cuprates may significantly affect the magnitudes of the mean-field and fluctuation intensity of DWO (e.g., γ_Δ, see Supplementary Note 6), which is an intriguing issue to be explored in the future.

A further interesting outcome is that the present energy law extends to the strange metal and superconductivity phases. The former comprises fluctuating vortices as an emergent dynamic order, characterized by the thermal de Broglie

wavelength ($l_T \propto T^{-1/2}$) or magnetic length ($l_B \propto B^{-1/2}$), which scatters carriers with a scattering rate inversely proportional to the square of these lengths[72]. The scattering rate also satisfies the energy law Eq. (1) with a linear dependence on temperature or magnetic field, consistent with recent experimental observations[53,72–74]. On the other hand, comprehensive measurements have demonstrated a universal linear relation between T_c and the superfluid density ρ_s in most doping regimes of hole-doped cuprates[75–77]. This indicates that the phase coherence energy $k_B T_c$ is inversely proportional to the square of the Cooper-pair distance ($l_p = \sqrt{\rho_s}$); thus, Eq. (4) is satisfied. Furthermore, Raman response measurements show that the nodal super-conducting gap Δ_{SC}^N has the same dome-like doping dependence on T_c[15], indicating $\Delta_{SC}^N \propto T_c \propto l_p^{-2}$, again satisfying Eq. (3).

Therefore, although originating from different microscopic mechanisms (e.g., the Umklapp scattering by DWO for pseudo-gap and strong phase fluctuations for superconductivity and strange metal), the characteristic energies (i.e., gap, transition temperature, and scattering rate) of the strange metal, pseudogap, and superconducting phases all satisfy an inverse square scaling on the characteristic lengths of mesoscopic orders (e.g., vortex, DWO, and Cooper pairs). This unified energy law reveals that, regardless of how complex the symmetry-broken forms are, a common invariance constrains the mesoscopic collective electronic motions in cuprates, providing a unified cross-scale link between the microscopic spectrum and macroscopic transport. We speculate that this invariance exhibits an intrinsic quantum nature of strongly correlated electrons and is worthy of further experimental verification and theoretical research in three directions:

First, it is interesting to verify the energy law for other strongly correlated materials, such as iron-based HTSC, iridate, organic, and heavy Fermion superconductors. Second, we suggest further explorations of the physical origin of the energy law to determine whether there is a local quantum wave state whose single-particle excitation is constrained by the period of a mesoscopic order and thus has quantum kinetic energy determined by the order's period, i.e., $E \propto h^2/m^* l_o^2$. It is highly plausible that the local quantum wave state and the unified energy law can be derived from an action of mesoscopic ordering (e.g., quantum XY model[5]) or the microscopic Hamiltonian (e.g., $t-J$ or Hubbard model) of correlated electrons through some renormalization calculations.

Finally, the present universality provides a clue for quantifying the intertwined behaviours of various forms of collective orders and fluctuations by considering the quantum coupling of multiple pairing or scattering channels. First of all, a thorough understanding of the pseudogap origin requires clarifying the intertwining relationship between the CDW and superconductivity. For instance, the comprehensive description of ARPES data at low and high-T regimes involves an intertwining of particle–particle and particle–hole pairing channels[78]. More interestingly, the recent Raman response measurements[14,15] found that the AN superconducting gap Δ_{SC}^{AN} is close to the CDW gap over a substantial doping range. Based on the present theory, it means that both gaps have a universal quadratic scaling with the CDW wavevector, i.e., $\Delta_{SC}^{AN} \sim \Delta_{CDW} \propto Q_{CDW}^2$. These universal energy laws provide an intriguing clue for advancing microscopic researches of the intertwining effects of particle–particle and particle–hole pairing channels[11,79]. Furthermore, many recent experiments observed that high magnetic fields suppress superconductivity to enhance or even induce CDW for cuprate compounds[57,80–87]. While the clarification of a specific microscopic mechanism for the origin of this field-induced CDW is beyond the scope of the present work, we

can offer a preliminary description for the field dependence of the magnetoresistance, consistent with the primary revelation of experimental observations, see Supplementary Note 7. On the other hand, the quantum coupling of multiple scattering channels will yield a comprehensive explanation for the preliminary observations that the total scattering rate can be expressed as a coupling formalism of multiple energy laws in recent experiments, e.g., $\sqrt{(k_B T)^2 + (\mu_B B)^2}$ [74,88,89], where μ_B is the Bohr magneton. The progress in these directions will significantly advance the understanding of non-Fermi liquids in strongly correlated electronic systems[90].

Methods

Characteristic energy scales and the DWO order parameter. In mean-field theory, the characteristic energies that determine the anomalous electronic spectrum and charge transport in the pseudogap phase are described by the single-particle self-energy, which, following Norman et al.'s theory[6], takes the following form:

$$\Sigma(\mathbf{k}, \omega) = \frac{\Delta_\mathbf{k}^2}{\omega \pm \epsilon_{\mathbf{k}+\mathbf{Q_o}} + i\Gamma_\mathbf{k}} - i\Gamma_\mathbf{k}, \tag{7}$$

where $\mathbf{k}$, ω, ϵ, and $\mathbf{Q_o}$ are the wavevector, frequency, and dispersion of a single-particle excitation and the DWO wavevector, respectively. Here, the anisotropic gap $\Delta_\mathbf{k}$ and the anisotropic scattering rate $\Gamma_\mathbf{k}$ are two critical energy scales describing the electron scattering by the mean-field effective potential and bosonic excitations of the fluctuating DWO (or impurities), respectively. This paper aims to uncover universal energy laws linking $\Delta_\mathbf{k}$ and $\Gamma_\mathbf{k}$ to the wavevector Q_o and the amplitude of the fluctuating DWO.

Generally, similar to electron–phonon scattering, the scattering energies in Eq. (7) is related to the real-space order parameters of the fluctuating DWO through the quasiparticle–phason scattering mechanism. To characterize the temporal fluctuations added to usual static DWO[17], we express the order parameter of the unidirectional DWO to be a space–time variable associated with a phase-averaged wavevector Q_o and the residual phase fluctuations $\phi(x,t)$ (ansatz no. 1):

$$\Psi(x, t) = A \exp[i(Q_o x + \phi(x, t))]. \tag{8}$$

Generally, phase fluctuations $\phi(x,t)$ can have any form. However, there is a special simple case, i.e., the plane wave mode with $\phi(x,t) = qx - \omega_q t$. For $\omega_q \neq 0$, the long-term average of the order parameter is zero, revealing that the order is fluctuating.

Umklapp scattering rate associated with DWO. This density wave (Eq. (8)) introduces an effective potential to scatter quasiparticles. Specifically, the corresponding carrier–phason interaction is proportional to the density wave modulations, i.e., $V = g_{DW} A \cos[Q_o x + \phi(x, t)]$, where g_{DW} is the carrier–DW coupling strength. Note that experimental evidence supported a strong coupling perspective of density wave instability in cuprates, which can be quantified by the $t-J$ model[11,91]. In this context, we introduce the ansatz no. 2 that the cuprate DWO can be described by the $t-J$ model, and the carrier–DW coupling strength is proportional to the superexchange energy, i.e., $g_{DW} \propto J$.

The energy law for the scattering rate (i.e., Eq. (1)) can be derived from a Umklapp scattering theory for phason modes of DWO[92], taking a small momentum difference and a long-wavelength approximation (ansatz no. 3). This scattering obeys the conservation of momentum as $\mathbf{k'} = \mathbf{k} + \mathbf{q} + n\mathbf{Q_o}$. For the characteristic energy of the mean scattering rate, Lee and Rice[92] predicted that:

$$\Gamma = 4\pi m^* \sum_{\mathbf{k},\mathbf{k'}} (\mathbf{v_{k'}} - \mathbf{v_k})^2 W_{\mathbf{k},\mathbf{k'}} \left[\delta(E_\mathbf{k} - E_{\mathbf{k'}} - \omega_\mathbf{q}) \frac{\partial f}{\partial E} \right.$$
$$\left. \times (1 + n_\mathbf{q} - f_{\mathbf{k'}}) + \delta(E_\mathbf{k} - E_{\mathbf{k'}} + \omega_\mathbf{q}) \frac{\partial f}{\partial E'} (1 + n_\mathbf{q} - f_\mathbf{k}) \right], \tag{9}$$

where $\mathbf{v}$ and E are the velocity and energy of a carrier, respectively; $\omega_\mathbf{q}$ is the frequency of the phason; and f and $n_\mathbf{q}$ are the distribution functions of the carrier and phason modes, respectively. Besides, $W_{\mathbf{k},\mathbf{k'}} = |\langle k'|V|k\rangle|^2 \propto A^2 J^2$ is the module square of the transition matrix element describing the carrier–phason scattering.

For a small momentum difference, it is reasonable to assume a linear relation, i.e., $(\mathbf{v_{k'}} - \mathbf{v_k}) \approx s\hbar(\mathbf{k} - \mathbf{k'})/m^*$, where s is a dimensionless constant. Furthermore, we assume that, compared to Q_o, the q of low-lying excitations is small, yielding $(\mathbf{v_{k'}} - \mathbf{v_k})^2 \approx n^2 s^2 \hbar^2 Q_o^2/(m^*)^2$. By substituting this expression into Eq. (9), we obtain Eq. (1) and a dimensionless coefficient describing the mean strength of

carrier–phason scattering:

$$\gamma_{\Gamma} = \frac{4}{\pi} n^2 s^2 \sum_{\mathbf{k'},\mathbf{k}} W_{\mathbf{k},\mathbf{k'}} \left[\delta(E_{\mathbf{k}} - E_{\mathbf{k'}} - \omega_{\mathbf{q}}) \frac{\partial f}{\partial E}(1 + n_{\mathbf{q}} - f_{\mathbf{k'}}) \right.$$
$$\left. + \delta(E_{\mathbf{k}} - E_{\mathbf{k'}} + \omega_{\mathbf{q}}) \frac{\partial f}{\partial E'}(1 + n_{\mathbf{q}} - f_{\mathbf{k}}) \right].$$

(10)

Finally, considering $\gamma_{\Gamma} \propto A^2 J^2$ is dimensionless, we can express it as $\gamma_{\Gamma} = F_{\Gamma} J^2 / t^2$ (i.e., the Eq. (2)) in the $t - J$ model, while the proportionality coefficient F_{Γ} includes the residual integral associated with electronic dispersions. The microscopic calculations of these electronic dispersions and integral beyond the scope of this work. Therefore, we introduce the ansatz no. 4 based on recent experimental observations[28,32,33], that is, we assume γ_{Γ} (and γ_{Δ}) in the pseudogap phase away from quantum critical points (and T^*) to be doping and temperature-independent and let the experimental data determine their magnitudes, see also discussions following Eq. (2).

Model the doping dependence of Q_{CDW}. To make continuous predictions dependence of the gap energy, the scattering rate, and the resistivity on doping, we propose a least-squares fit for the doping-dependent phase-averaged Q_{CDW} data. During the fitting procedure, we assume that the amplitude of the fluctuating CDW is nonzero in the doping range considered in this work. Under the constraints of simplicity and physical consistency, we found that the linear fit and the defect power law are the two most suitable fitting functions for Hg-1201, Bi-2212, and Bi-2201, as shown in Supplementary Fig. 1 (see Supplementary Note 1). For instance, although a polynomial provides a more accurate fit for Q_{CDW} of Bi-2201, it is inconsistent with the observation that the CDW is nearly commensurate in the lightly doped Bi-2201[21,24]. In contrast, a defect power law, i.e., $Q_{CDW} = 0.269[1 - (p/0.261)^{3.79}]$, is the simplest function consistent with this scenario.

The choice of validating samples. To date, there have been thousands of reported experimental measurements devoted to the pseudogap, DWO, and resistivity, involving considerable diversity, compound series, doping regimes, and sample qualities. To identify a universal energy law, we restrict ourselves mainly to high-quality single crystals with short-range DWO to remove various higher-order effects, e.g., excessive impurities and the long-range ordering effect. Therefore, in this paper, the samples selected for validation are high-quality single-crystal series of hole-doped Bi-2201, Bi-2212, and Hg-1201 prepared by highly respected experimental groups for their strong two-dimensional nature and systematic observations of short-range DWO[14,15,27,40,44], as well as the lowest reported resistivity values among all reported data associated with the same compound (e.g., Bi-2201 prepared by Ando's group[48,52]). Therefore, the choice of our validating samples is not arbitrary but consistent with our strict theoretical requirements. Please refer to Supplementary Notes 4 and 5 for the corresponding list of the data sources used in this work.

Data availability

All experimental data analysed and presented in the main text and supplementary materials can be found in an online repository https://github.com/luhaozhang/Validation-for-unified-energy-law-in-pseudogap-phase.git. Further material is available from the corresponding author upon reasonable request.

Code availability

All code utilized in the simulations presented in the main text and supplementary text can be found in an online repository https://github.com/luhaozhang/Validation-for-unified-energy-law-in-pseudogap-phase.git. Further material is available from the corresponding author upon reasonable request.

References

1. Keimer, B., Kivelson, S. A., Norman, M. R., Uchida, S. & Zaanen, J. From quantum matter to high-temperature superconductivity in copper oxides. *Nature* **518**, 179–186 (2015).
2. Kordyuk, A. A. Pseudogap from ARPES experiment: three gaps in cuprates and topological superconductivity. *Low Temp. Phys.* **41**, 319–341 (2015).
3. Frano, A., Blanco-Canosa, S., Keimer, B. & Birgeneau, R. J. Charge ordering in superconducting copper oxides. *J. Phys. Condens. Matter* **32**, 374005 (2020).
4. Sato, Y. et al. Thermodynamic evidence for a nematic phase transition at the onset of the pseudogap in YBa$_2$Cu$_3$O$_y$. *Nat. Phys.* **13**, 1074–1078 (2017).
5. Varma, C. M. Colloquium: Linear in temperature resistivity and associated mysteries including high temperature superconductivity. *Rev. Mod. Phys.* **92**, 031001 (2020).
6. Norman, M. R., Kanigel, A., Randeria, M., Chatterjee, U. & Campuzano, J. C. Modeling the Fermi arc in underdoped cuprates. *Phys. Rev. B* **76**, 174501 (2007).
7. Sebastian, S. E. & Proust, C. Quantum oscillations in hole-doped cuprates. *Annu. Rev. Condens. Matter Phys.* **6**, 411–430 (2015).
8. Agterberg, D. F. et al. The physics of pair-density waves: cuprate superconductors and beyond. *Annu. Rev. Condens. Matter Phys.* **11**, 231–270 (2020).
9. Varma, C. M. Pseudogap and Fermi arcs in underdoped cuprates. *Phys. Rev. B* **99**, 224516 (2019).
10. Uchida, S. Identifying the pseudogap in cuprates with a nematic phase. *J. Phys. Soc. Jpn.* **17**, 07 (2020).
11. Fradkin, E., Kivelson, S. A. & Tranquada, J. M. Colloquium: theory of intertwined orders in high temperature superconductors. *Rev. Mod. Phys.* **87**, 457–482 (2015).
12. Fernandes, R. M., Orth, P. P. & Schmalian, J. Intertwined vestigial order in quantum materials: nematicity and beyond. *Annu. Rev. Condens. Matter Phys.* **10**, 133–154 (2019).
13. Nie, L., Maharaj, A. V., Fradkin, E. & Kivelson, S. A. Vestigial nematicity from spin and/or charge order in the cuprates. *Phys. Rev. B* **96**, 085142 (2017).
14. Loret, B. et al. Intimate link between charge density wave, pseudogap and superconducting energy scales in cuprates. *Nat. Phys.* **15**, 771–775 (2019).
15. Loret, B. et al. Universal relationship between the energy scales of the pseudogap phase, the superconducting state, and the charge-density-wave order in copper oxide superconductors. *Phys. Rev. B* **101**, 214520 (2020).
16. Mukhopadhyay, S. et al. Evidence for a vestigial nematic state in the cuprate pseudogap phase. *Proc. Natl Acad. Sci. USA* **116**, 13249–13254 (2019).
17. Mesaros, A. et al. Commensurate $4a_0$-period charge density modulations throughout the Bi$_2$Sr$_2$CaCu$_2$O$_{8+x}$ pseudogap regime. *Proc. Natl Acad. Sci. USA* **113**, 12661–12666 (2016).
18. Zhao, H. et al. Charge-stripe crystal phase in an insulating cuprate. *Nat. Mater.* **18**, 103–107 (2019).
19. Zhang, Y. et al. Machine learning in electronic-quantum-matter imaging experiments. *Nature* **570**, 484–490 (2019).
20. Vinograd, I. et al. Locally commensurate charge-density wave with three-unit-cell periodicity in YBa$_2$Cu$_3$O$_y$. *Nat. Commun.* **12**, 3274 (2021).
21. Webb, T. A. et al. Density wave probes cuprate quantum phase transition. *Phys. Rev. X* **9**, 021021 (2019).
22. Kivelson, S. A. & Lederer, S. Linking the pseudogap in the cuprates with local symmetry breaking: a commentary. *Proc. Natl Acad. Sci. USA* **116**, 14395–14397 (2019).
23. Fujita, M. et al. Progress in neutron scattering studies of spin excitations in high-T_c cuprates. *J. Phys. Soc. Jpn.* **81**, 011007 (2012).
24. Cai, P. et al. Visualizing the evolution from the Mott insulator to a charge-ordered insulator in lightly doped cuprates. *Nat. Phys.* **12**, 1047–1051 (2016).
25. She, Z. S., Chen, X. & Hussain, F. Quantifying wall turbulence via a symmetry approach: a Lie group theory. *J. Fluid Mech.* **827**, 322–356 (2017).
26. Chen, X., Hussain, F. & She, Z. S. Quantifying wall turbulence via a symmetry approach. Part 2. Reynolds stresses. *J. Fluid Mech.* **850**, 401–438 (2018).
27. Comin, R. & Damascelli, A. Resonant X-ray scattering studies of charge order in cuprates. *Annu. Rev. Condens. Matter Phys.* **7**, 369–405 (2016).
28. Arpaia, R. et al. Dynamical charge density fluctuations pervading the phase diagram of a Cu-based high-T_c superconductor. *Science* **365**, 906–910 (2019).
29. Lee, P. A., Nagaosa, N. & Wen, X. G. Doping a Mott insulator: physics of high-temperature superconductivity. *Rev. Mod. Phys.* **78**, 17–85 (2006).
30. Hybertsen, M. S., Stechel, E. B., Schluter, M. & Jennison, D. R. Renormalization from density-functional theory to strong-coupling models for electronic states in Cu–O materials. *Phys. Rev. B* **41**, 11068–11072 (1990).
31. Sulewski, P. E., Fleury, P. A., Lyons, K. B., Cheong, S. W. & Fisk, Z. Light scattering from quantum spin fluctuations in R$_2$CuO$_4$(R = La, Nd, Sm). *Phys. Rev. B* **41**, 225–230 (1990).
32. Yu, B. et al. Unusual dynamic charge correlations in simple-tetragonal HgBa$_2$CuO$_{4+\delta}$. *Phys. Rev. X* **10**, 021059 (2020).
33. Peng, Y. Y. et al. Dispersion, damping, and intensity of spin excitations in the monolayer (Bi,Pb)$_2$(Sr,La)$_2$CuO$_{6+\delta}$ cuprate superconductor family. *Phys. Rev. B* **98**, 144507 (2018).
34. Wang, Y. & Chubukov, A. Charge-density-wave order with momentum (2Q, 0) and (0, 2Q) within the spin-fermion model: continuous and discrete symmetry breaking, preemptive composite order, and relation to pseudogap in hole-doped cuprates. *Phys. Rev. B* **90**, 035149 (2014).
35. Yoshida, T. et al. Coexistence of a pseudogap and a superconducting gap for the high-T_c superconductor La$_{2-x}$Sr$_x$CuO$_4$ studied by angle-resolved photoemission spectroscopy. *Phys. Rev. B* **93**, 014513 (2016).
36. Dai, Y. M. et al. Doping evolution of the optical scattering rate and effective mass of Bi$_2$Sr$_{2-x}$La$_x$CuO$_6$. *Phys. Rev. B* **85**, 092504 (2012).
37. Comin, R. et al. Charge order driven by Fermi-arc instability in Bi$_2$Sr$_{2-z}$La$_z$CuO$_{6+\delta}$. *Science* **343**, 390–392 (2014).

38. Wise, W. D. et al. Imaging nanoscale Fermi-surface variations in an inhomogeneous superconductor. *Nat. Phys.* **5**, 213–216 (2009).

39. Barišić, N. et al. Universal quantum oscillations in the underdoped cuprate superconductors. *Nat. Phys.* **9**, 761–764 (2013).

40. Tabis, W. et al. Synchrotron x-ray scattering study of charge-density-wave order in $HgBa_2CuO_{4+\delta}$. *Phys. Rev. B* **96**, 134510 (2017).

41. Campi, G. et al. Inhomogeneity of charge-density-wave order and quenched disorder in a high-T_c superconductor. *Nature* **525**, 359–362 (2015).

42. Campuzano, J. C. et al. Electronic spectra and their relation to the (π, π) collective mode in high-T_c superconductors. *Phys. Rev. Lett.* **83**, 3709–3712 (1999).

43. He, Y. et al. Fermi surface and pseudogap evolution in a cuprate superconductor. *Science* **344**, 608–611 (2014).

44. Peng, Y. Y. et al. Re-entrant charge order in overdoped $(Bi,Pb)_{2.12}Sr_{1.88}CuO_{6+\delta}$ outside the pseudogap regime. *Nat. Mater.* **17**, 697–702 (2018).

45. Chakravarty, S., Laughlin, R. B., Morr, D. K. & Nayak, C. Hidden order in the cuprates. *Phys. Rev. B* **63**, 094503 (2001).

46. Yang, K. Y., Rice, T. M. & Zhang, F. C. Phenomenological theory of the pseudogap state. *Phys. Rev. B* **73**, 174501 (2006).

47. Abrahams, E. & Varma, C. M. What angle-resolved photoemission experiments tell about the microscopic theory for high-temperature superconductors. *Proc. Natl Acad. Sci. USA* **97**, 5714–5716 (2000).

48. Ando, Y., Komiya, S., Segawa, K., Ono, S. & Kurita, Y. Electronic phase diagram of high-T_c cuprate superconductors from a mapping of the in-plane resistivity curvature. *Phys. Rev. Lett.* **93**, 267001 (2004).

49. Ono, S. et al. Metal-to-insulator crossover in the low-temperature normal state of $Bi_2Sr_{2-x}La_xCuO_{6+\delta}$. *Phys. Rev. Lett.* **85**, 638–641 (2000).

50. Legros, A. et al. Universal T-linear resistivity and Planckian dissipation in overdoped cuprates. *Nat. Phys.* **15**, 142–147 (2019).

51. Zaanen, J. Why the temperature is high. *Nature* **430**, 512–513 (2004).

52. Ando, Y. et al. Carrier concentrations in $Bi_2Sr_{2-z}La_zCuO_{6+\delta}$ single crystals and their relation to the Hall coefficient and thermopower. *Phys. Rev. B* **61**, R14956–R14959 (2000).

53. Giraldo-Gallo, P. et al. Scale-invariant magnetoresistance in a cuprate superconductor. *Science* **361**, 479–481 (2018).

54. Kasahara, S. et al. Evolution from non-Fermi- to Fermi-liquid transport via isovalent doping in $BaFe_2(As_{1-x}P_x)_2$ superconductors. *Phys. Rev. B* **81**, 184519 (2010).

55. Goldman, A. M. Superconductor–insulator transitions. *Int. J. Mod. Phys. B* **24**, 4081–4101 (2010).

56. Wen, J. J. et al. Observation of two types of charge-density-wave orders in superconducting $La_{2-x}Sr_xCuO_4$. *Nat. Commun.* **10**, 3269 (2019).

57. Kawasaki, S. et al. Charge-density-wave order takes over antiferromagnetism in $Bi_2Sr_{2-x}La_xCuO_6$ superconductors. *Nat. Commun.* **8**, 1267 (2017).

58. Hashimoto, M., Vishik, I. M., He, R. H., Devereaux, T. P. & Shen, Z. X. Energy gaps in high-transition-temperature cuprate superconductors. *Nat. Phys.* **10**, 483–495 (2014).

59. Miao, H. et al. Charge density waves in cuprate superconductors beyond the critical doping. *npj Quantum Mater.* **6**, 31 (2021).

60. Grbić, M. S. et al. Temperature range of superconducting fluctuations above T_c in $YBa_2Cu_3O_{7-\delta}$ single crystals. *Phys. Rev. B* **83**, 144508 (2011).

61. Grbić, M. S. et al. Microwave measurements of the in-plane and c-axis conductivity in $HgBa_2CuO_{4+\delta}$: discriminating between superconducting fluctuations and pseudogap effects. *Phys. Rev. B* **80**, 094511 (2009).

62. Sarkar, T. et al. Fermi surface reconstruction and anomalous low-temperature resistivity in electron-doped $La_{2-x}Ce_xCuO_4$. *Phys. Rev. B* **96**, 155449 (2017).

63. Moon, S. J. et al. Dimensionality-controlled insulator–metal transition and correlated metallic state in 5d transition metal oxides $Sr_{n+1}Ir_nO_{3n+1}$ ($n = 1, 2,$ and infinity). *Phys. Rev. Lett.* **101**, 226402 (2008).

64. Battisti, I. et al. Universality of pseudogap and emergent order in lightly doped mott insulators. *Nat. Phys.* **13**, 21–25 (2017).

65. Miao, H. et al. Formation of incommensurate charge density waves in cuprates. *Phys. Rev. X* **9**, 031042 (2019).

66. Lin, J. Q. et al. Strongly correlated charge density wave in $La_{2-x}Sr_xCuO_4$ evidenced by doping-dependent phonon anomaly. *Phys. Rev. Lett.* **124**, 207005 (2020).

67. Miao, H. et al. High-temperature charge density wave correlations in $La_{1.875}Ba_{0.125}CuO_4$ without spin-charge locking. *Proc. Natl Acad. Sci. USA* **114**, 12430–12435 (2017).

68. Miao, H. et al. Incommensurate phonon anomaly and the nature of charge density waves in cuprates. *Phys. Rev. X* **8**, 011008 (2018).

69. Blanco-Canosa, S. et al. Resonant x-ray scattering study of charge-density wave correlations in $YBa_2Cu_3O_{6+x}$. *Phys. Rev. B* **90**, 054513 (2014).

70. Ando, Y. et al. Metallic in-plane and divergent out-of-plane resistivity of a high-T_c cuprate in the zero-temperature limit. *Phys. Rev. Lett.* **77**, 2065–2068 (1996).

71. Meng, J. et al. Growth, characterization and physical properties of high-quality large single crystals of $Bi_2Sr_{2-x}La_xCuO_6$ high-temperature superconductors. *Supercond. Sci. Technol.* **22**, 045010 (2009).

72. Li, R. & She, Z. S. Emergent mesoscopic quantum vortex and Planckian dissipation in the strange metal phase. *New J. Phys.* **23**, 043050 (2021).

73. Bruin, J. A. N., Sakai, H., Perry, R. S. & Mackenzie, A. P. Similarity of scattering rates in metals showing T-linear resistivity. *Science* **339**, 804–807 (2013).

74. Hayes, I. M. et al. Scaling between magnetic field and temperature in the high-temperature superconductor $BaFe_2(As_{1-x}P_x)_2$. *Nat. Phys.* **12**, 916–919 (2016).

75. Uemura, Y. J. et al. Universal correlations between T_c and n_s/m^* (carrier density over effective mass) in high-T_c cuprate superconductors. *Phys. Rev. Lett.* **62**, 2317–2320 (1989).

76. Božović, I., He, X., Wu, J. & Bollinger, A. T. Dependence of the critical temperature in overdoped copper oxides on superfluid density. *Nature* **536**, 309–311 (2016).

77. Božović, I., He, X., Wu, J. & Bollinger, A. T. The vanishing superfluid density in cuprates-and why it matters. *J. Supercond. Nov. Magn.* **31**, 2683–2690 (2018).

78. He, R. H. et al. From a single-band metal to a high-temperature superconductor via two thermal phase transitions. *Science* **331**, 1579–1583 (2011).

79. Lee, P. A. Amperean pairing and the pseudogap phase of cuprate superconductors. *Phys. Rev. X* **4**, 031017 (2014).

80. Wu, T. et al. Magnetic-field-induced charge-stripe order in the high-temperature superconductor $YBa_2Cu_3O_y$. *Nature* **477**, 191–194 (2011).

81. Wu, T. et al. Emergence of charge order from the vortex state of a high-temperature superconductor. *Nat. Commun.* **4**, 2113 (2013).

82. Chang, J. et al. Magnetic field controlled charge density wave coupling in underdoped $YBa_2Cu_3O_{6+x}$. *Nat. Commun.* **7**, 11494 (2016).

83. Jang, H. et al. Ideal charge-density-wave order in the high-field state of superconducting YBCO. *Proc. Natl Acad. Sci. USA* **113**, 14645–14650 (2016).

84. Machida, T. et al. Bipartite electronic superstructures in the vortex core of $Bi_2Sr_2CaCu_2O_{8+\delta}$. *Nat. Commun.* **7**, 11747 (2016).

85. Kacmarcik, J. et al. Unusual Interplay between superconductivity and field-induced charge order in $YBa_2Cu_3O_y$. *Phys. Rev. Lett.* **121**, 167002 (2018).

86. Edkins, S. D. et al. Magnetic field-induced pair density wave state in the cuprate vortex halo. *Science* **364**, 976–980 (2019).

87. Choi, J. et al. Spatially inhomogeneous competition between superconductivity and the charge density wave in $YBa_2Cu_3O_{6.67}$. *Nat. Commun.* **11**, 990 (2020).

88. Licciardello, S. et al. Coexistence of orbital and quantum critical magnetoresistance in $FeSe_{1-x}S_x$. *Phys. Rev. Res.* **1**, 023011 (2019).

89. Nakajima, Y. et al. Quantum-critical scale invariance in a transition metal alloy. *Commun. Phys.* **3**, 181 (2020).

90. Lee, S. S. Recent developments in non-Fermi liquid theory. *Annu. Rev. Condens. Matter Phys.* **9**, 227–244 (2018).

91. Kivelson, S. A. et al. How to detect fluctuating stripes in the high-temperature superconductors. *Rev. Mod. Phys.* **75**, 1201–1241 (2003).

92. Lee, P. A. & Rice, T. M. Electric field depinning of charge density waves. *Phys. Rev. B* **19**, 3970–3980 (1979).

93. Zhou, W. & Liang, W. *Fundamental Research of High-Temperature Superconductor* (Shanghai Science Press, Shanghai, 1999).

94. Wen, H. H. et al. Specific-heat measurement of a residual superconducting state in the normal state of underdoped $Bi_2Sr_{2-x}La_xCuO_{6+\delta}$ cuprate superconductors. *Phys. Rev. Lett.* **103**, 067002 (2009).

95. Komiya, S., Chen, H., Zhang, S. & Ando, Y. Magic doping fractions for high-temperature superconductors. *Phys. Rev. Lett.* **94**, 207004 (2005).

96. Mandrus, D., Forro, L., Kendziora, C. & Mihaly, L. Two-dimensional electron localization in bulk single crystals of $Bi_2Sr_2Y_xCa_{1-x}Cu_2O_8$. *Phys. Rev. B* **44**, 2418–2421 (1991).

97. Orgiani, P. et al. Direct measurement of sheet resistance Rsquare in cuprate systems: evidence of a fermionic scenario in a metal–insulator transition. *Phys. Rev. Lett.* **98**, 036401 (2007).

98. Rullier-Albenque, F., Colson, D., Forget, A., Thuéry, P. & Poissonnet, S. Hole and electron contributions to the transport properties of $Ba(Fe_{1-x}Ru_x)_2As_2$ single crystals. *Phys. Rev. B* **81**, 224503 (2010).

99. Shi, Z., Baity, P. G., Sasagawa, T. & Popovic, D. Vortex phase diagram and the normal state of cuprates with charge and spin orders. *Sci. Adv.* **6**, aay8946 (2020).

100. Rullier-Albenque, F. Influence of the electronic structure on the transport properties of some iron pnictides. *C. R. Phys.* **17**, 164–187 (2016).

101. Ye, Z. R. et al. Doping dependence of the electronic structure in phosphorus-doped ferropnictide superconductor $BaFe_2(As_{1-x}P_x)_2$ studied by angle-resolved photoemission spectroscopy. *Phys. Rev. B* **86**, 035136 (2012).

102. Sawa, A., Kawasaki, M., Takagi, H. & Tokura, Y. Electron-doped superconductor $La_{2-x}Ce_xCuO_4$: preparation of thin films and modified doping range for superconductivity. *Phys. Rev. B* **66**, 014531 (2002).

Acknowledgements

Author contributions

Both authors conceived the original idea and wrote the paper. Z.S. supervised the project. R.L. performed the data analysis.

Competing interests

The authors declare no competing interests.

Additional information

Supplementary information The online version contains supplementary material available at https://doi.org/10.1038/s42005-021-00789-9.

Correspondence and requests for materials should be addressed to Zhen-Su She.

Peer review information *Communications Physics* thanks Debmalya Chakraborty and the other, anonymous, reviewer(s) for their contribution to the peer review of this work. Peer reviewer reports are available.

Reprints and permission information is available at http://www.nature.com/reprints

Publisher's note Springer Nature remains neutral with regard to jurisdictional claims in published maps and institutional affiliations.